Journal of Magnetic Resonance **155,** 64–71 (2002)
doi:10.1006/jmre.2002.2516, available online at http://www.idealibrary.com on IDEAL®

^{1}H Detected ^{13}C Echo Planar Imaging

Alex. M. J. Hudson,* Walter Köckenberger,* Michael Heidenreich,† Narayanan Chandrakumar,‡ Rainer Kimmich,† and Richard Bowtell*

*Magnetic Resonance Centre, School of Physics and Astronomy, University of Nottingham, University Park, Nottingham NG7 2RD, United Kingdom; †Sektion Kernresonanzspektroskopie, Universität Ulm, 89069 Ulm, Germany; and ‡Department of Chemistry, Indian Institute of Technology Madras, Chennai 600 036, Tamil Nadu, India

Received August 13, 2001; revised December 18, 2001

Cyclic *J* cross polarisation (CYCLCROP) is a sensitive method for the noninvasive monitoring of ^{13}C distributions and fluxes. The PRAWN rotating frame Hartmann-Hahn mixing sequence ameliorates problems associated with sensitivity to Hartmann-Hahn mismatch and reduces RF power deposition. The combination of CYCLCROP with echo planar imaging (EPI) for spatial encoding of the proton detected carbon signal allows efficient use of the available signal to be made, permitting a significant improvement in the temporal resolution of any study. We report here on some initial experiments to demonstrate the feasibility of echo planar proton detected ^{13}C imaging using CYCLCROP based upon the PRAWN module, including the application of the technique to the measurement of transport and accumulation of ^{13}C-labelled sucrose in a castor bean seedling. Two methods that can be used to eliminate the effect of the *J*-splitting in the EP images are presented. In addition, a fast, image-based B_1 field-mapping method which may be used to quantitatively map the low frequency RF field in a dual resonant (^{13}C/^{1}H) probe is presented. The technique utilises the above described imaging method, permitting fully quantitative, 64×64 axial field maps to be generated in about a minute.

Key Words: **polarization transfer; CYCLCROP; PRAWN; EPI; B_1-field mapping.**

INTRODUCTION

The utility of direct ^{13}C NMR spectroscopy has been demonstrated in a wide variety of applications (*1*) including investigations of metabolism, biochemical analysis, elucidation of protein structures, and studies in polymer sciences. In many of these applications, however, the technique offers insufficient sensitivity to allow the detection of ^{13}C compounds at low concentrations or the monitoring of dynamic processes with adequate temporal resolution. The significant sensitivity enhancement provided by indirect detection of the ^{13}C nucleus is thus of considerable utility. Using the cyclic *J* cross polarization (CYCLCROP) (*2*) technique, the ^{13}C nucleus can be detected with almost the same sensitivity as a comparable number of ^{1}H nuclei, leading to a theoretical increase of the signal of $(\gamma^{1H}/\gamma^{13C})^3 = 64$, as compared to a direct ^{13}C one-pulse experiment (*3*). Further gains in sensitivity per unit time may also be realized with this technique by taking advantage of the faster repetition rates allowed by the lower relaxation times of ^{1}H nuclei compared with those of ^{13}C. The improvement in sensitivity delivered by the CYCLCROP technique permits proton-detected ^{13}C-images to be acquired in much reduced times, even at natural abundance or at low ^{13}C enrichment (*4*). For example, the movement of ^{13}C-labeled metabolites has been mapped in small plants using CYCLCROP in conjunction with short-echo-time spin-warp imaging with a temporal resolution of 100 min and a voxel volume of 0.3 mm^3 at 9.4 T (*5*). The CYCLCROP approach maintains a high degree of spectral selectivity. In previous *in vitro* work (*5*) carried out on a mixture of ^{13}C-labeled fructose and sucrose at 9.4 T it was possible to detect selectively the signal from either the C1 molecular group of fructose ($\delta(^{13}C) = 64.8$ ppm, $\delta(^{1}H) = 3.63$ ppm) or the F1 resonance of the sucrose molecule ($\delta(^{13}C) = 62.3$ ppm, $\delta(^{1}H) = 3.56$ ppm).

A possible route toward speeding up indirect detected imaging techniques is to make more efficient use of the edited proton signal. Using a reduced interexperimental delay and low flip angle excitation, as employed in fast gradient echo imaging techniques (*6*), is, however, not a viable approach in this context, since CYCLCROP leads to complete saturation of the ^{1}H magnetization after each signal acquisition. Another approach is to multiply refocus the edited ^{1}H signal and thus sample multiple lines of *k*-space after each polarization transfer (*7*). The CYCLCROP echo-planar imaging (EPI) sequence described here involves taking this approach to the extreme, such that all lines of *k*-space are acquired after each transfer. In samples with reasonable T_2^* relaxation times this sequence provides the optimal signal to noise ratio (SNR) per unit time (*8*). In situations where the concentration of ^{13}C is high, such that adequate image SNR can be achieved in a small number of signal acquisitions, the CYCLCROP-EPI sequence can also provide improved temporal resolution for monitoring dynamic processes, compared with spin-warp acquisition. For lower concentrations of ^{13}C such that the minimum time to acquire echo-planar images with adequate SNR is greater than the time that it takes to acquire all the required phase encodes of a spin-warp image this feature of echo-planar image acquisition is not advantageous, and both types of image can be acquired with the same SNR. However, the acquisition of all lines in *k*-space after a single

1090-7807/02 $35.00

"excitation" in EPI means that movement or changes in the signal in a long experiment during which multiple averages are acquired only cause image blurring, whereas in spin-warp acquisition such effects will cause artefacts that may propagate throughout the whole image. These attributes of the echo-planar-based sequence may be particularly advantageous in metabolic studies on animals and humans, where images with coarse spatial resolution, but reasonable temporal resolution can provide useful information. Extrapolating from previous human studies (*9*) carried out at 4 T using optimized hardware, in which 0.67 μmol of ^{13}C (^{13}C natural abundance N-acetyl aspartate in a 12-cm^3 localized volume) was detected using proton-observe-carbon-edited spectroscopy (POCE) (*10*) with an SNR of 13 in 6 min, detection of 2 mM ^{13}C-labeled metabolite using CYCLCROP EPI with 1 cm^3 voxel size, and SNR of greater than 10 should be possible in a few minutes. The combination of CYCLCROP and EPI does, however, pose some particular technical challenges, mainly relating to the effect of the ^{13}C–^{1}H J-coupling on the evolution of the signal during the EPI acquisition.

Here we describe initial experiments showing the feasibility of combining CYCLCROP and EPI in experiments carried out at 11.7 and 9.4 T using a pulsed variant of the rotating frame polarization transfer method (*11*). Two alternative methods of eliminating the effect of J-coupling during echo-planar image acquisition are also introduced in Methods. The application of the technique to monitoring the transport and accumulation of ^{13}C-labeled sucrose in the vascular bundles of a castor bean seedling (*Ricinus communis* L.) and to rapid mapping of the B_1 homogeneity of RF coils tuned to the ^{13}C NMR frequency is also detailed.

^{1}H detected ^{13}C imaging based on the use of echo-planar spectroscopic imaging (*12*) has been described previously (*13, 14*). Hyder *et al.* (*13*) implemented ^{1}H echo-planar spectroscopic imaging in conjunction with the POCE editing method (*10*) at 7 T and used this approach to monitor the regional [4-^{13}CH$_2$] glutamate turnover in rat brain. Morikawa and Inubushi (*14*) have used a similar imaging method in conjunction with a ^{1}H detected ^{13}C gradient-enhanced heteronuclear multiple quantum coherence sequence to map the distribution of [1-^{13}C] glucose and metabolic products in rat brain at 2 T. The sequences employed in this previous work differ from that described here in both the methods used to achieve polarization transfer and the imaging sequence employed. Spectroscopic imaging is necessary when the edited ^{1}H signal is produced by nuclei in more than one chemical group. The echo-planar spectroscopic imaging sequence uses a single rapidly switched gradient to generate an echo train, Fourier transformation of which yields a set of spectra that are spatially resolved in one dimension. Generation of spectra resolved in two spatial dimensions requires that the experiment be repeated and an incremented phase-encode gradient applied. In the work described here, the high spectral selectivity of CYCLCROP leads to the generation of ^{1}H signals only from a single type of coupled spin. With the methods for suppressing the effects of J-coupling which we describe here, this allows imaging to be carried out using a standard echo-planar acquisition, without the need for phase-encoding.

METHODS

The CYCLCROP–EPI Implementation

The cyclic polarization transfer sequence, CYCLCROP (*3*), for the generation of carbon-edited proton signal may be summarized as follows (Fig. 1). After an initial ^{1}H excitation pulse, a polarization transfer module generates enhanced ^{13}C magnetization in a selected group of ^{1}H and ^{13}C nuclei. The application of a ^{13}C, 90° RF pulse stores the resulting magnetization along the z-axis. A comb of 90°, ^{1}H excitation pulses, interspersed

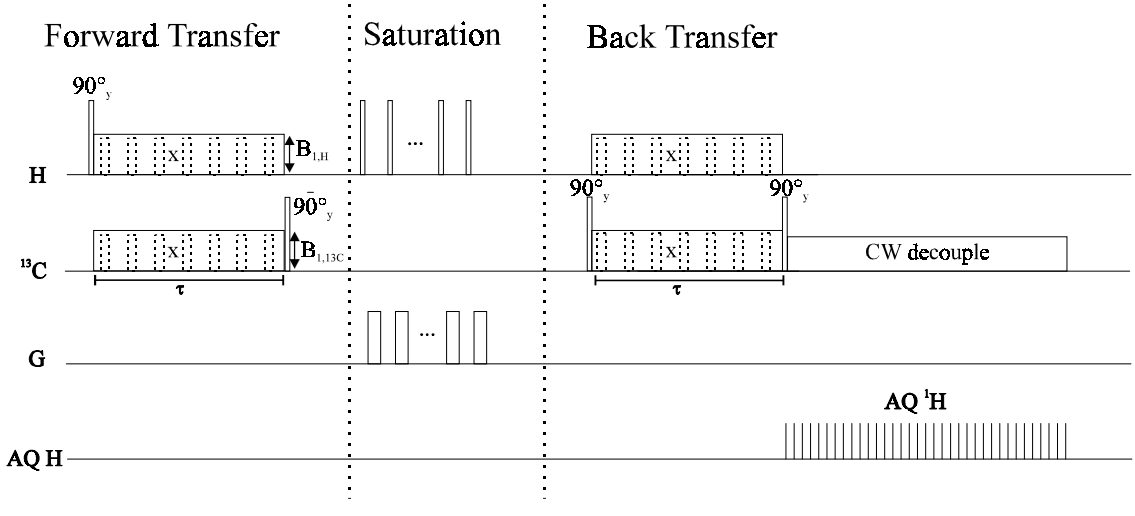

FIG. 1. Schematic diagram of the CYCLCROP pulse sequence (using cyclic J-cross polarization) followed by detection of a decoupled ^{1}H signal. The RF pulses used in the alternative, PRAWN cross polarization module are shown as dotted lines.

with crusher gradients, then saturates all noncoupled protons, before the stored ^{13}C magnetization is read back with a further ^{13}C, 90° RF "recall" pulse. A second polarization transfer module then restores the magnetization of only the ^{1}H nuclei that are J-coupled to appropriate ^{13}C nuclei. The ^{13}C-edited ^{1}H NMR signal may then be read out under continuous wave decoupling to yield a singlet in a spectroscopic experiment. Imaging can be accomplished by spatially encoding the edited signal in the usual manner.

A new polarization transfer module, known as PRAWN (Pulsed Rotating frame trAnsfer sequence with WiNdows), was recently introduced by Chandrakumar and Kimmich (*11*). In this module, the continuous wave (CW) spin-lock and contact pulses of the original Hartmann–Hahn experiment are split up into a series of small flip angle pulses, whose rotations typically add to a multiple of 360° and which are interspersed with free evolution "windows," as shown in Fig. 1. It can be shown by the use of average Hamiltonian theory that the effective Hamiltonian of this pulse sequence is of a form similar to that describing the conventional CW Hartmann–Hahn sequence (*11*). Polarization transfer is therefore achieved when the pulsed RF fields obey the Hartmann–Hahn matching condition and the duration of the PRAWN module is the same as that required in the CW method (e.g., a time of J^{-1} for an IS spin system). However, the PRAWN module has the significant advantage of a reduced sensitivity to Hartmann–Hahn mismatch compared to that of the CW sequence at fixed B_1 amplitude (*11*). The PRAWN module thus yields efficient polarization transfer at lower specific absorption rates (SAR) than the CW approach, while maintaining an acceptable sensitivity to frequency offsets as is fully described in Ref. (*11*). The PRAWN method was therefore employed in the experiments described in this paper.

The particular implementation of PRAWN employed twenty 18° RF pulses ($\frac{\gamma B_1}{2\pi} = 1$ kHz). The total duration of the PRAWN module, τ, was adjusted to the optimal contact time for the specific J-coupling constant in each case, giving a typical RF duty cycle during the PRAWN module of 20–29%. The saturation of the ^{1}H magnetization between the forward and reverse polarization transfers was achieved via the application of a single 4-ms, 2.6-kHz sin/cos adiabatic half passage (*15*) and three B_1-inhomogeneity-compensating composite pulses (*16*), interspersed with spoiler gradient pulses. The areas of these gradient pulses followed a geometric progression (decreasing in size), thus avoiding refocusing of any unwanted coherences. A 90°, ^{13}C RF pulse at the end of the second polarization transfer module was used to eliminate any anti-phase signal components, which inherently arise during the polarization transfer in $I_N S$ spin systems with $N \geq 2$ (*17, 18*).

Spatial encoding of the edited ^{1}H signal was accomplished using a spin–echo MBEST EPI sequence (*19*) as shown in Fig. 2. Slice selection was achieved using a selective 180° RF pulse to generate the spin echo. Typically 64 echoes were acquired with a time per echo of 0.9 ms, leading to an echo-train of duration 58 ms. Under the effect of the coupling Hamiltonian for scalar

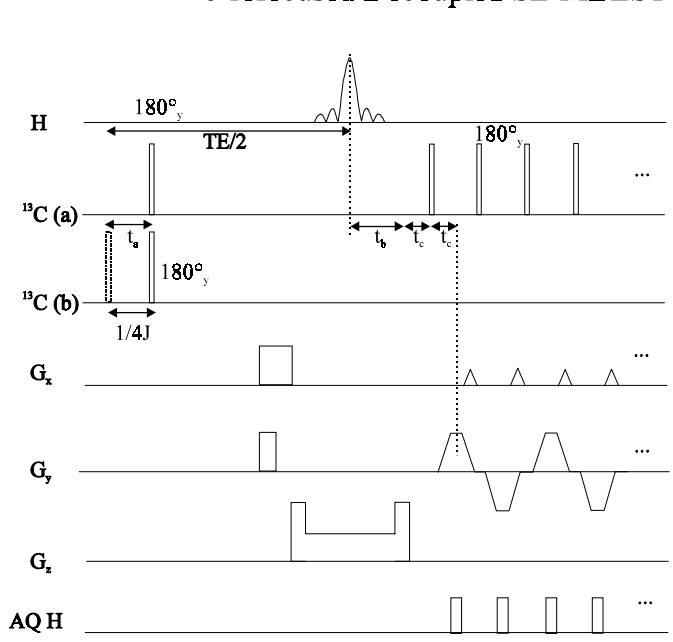

FIG. 2. EPI sequence used for imaging the signal formed after the CYCLROP procedure. Two schemes for eliminating the effect of ^{13}CH J-coupling during the EPI signal acquisition are indicated on the ^{13}C RF channel. In (a), 180° RF pulses are applied at the zero crossings of the oscillating read gradient. In (b), two images are acquired with a single ^{13}C, 180° RF pulse applied so as to generate in-phase (dotted line pulse, applied immediately after the end of the CYCLCROP module) and anti-phase (solid line pulse, shifted by a time $1/4J$ from the end of the CYCLCROP module) signal from the two components of the doublet.

coupled $I_N S$ spin systems, the proton resonance forms an in-phase doublet with a splitting of J. In spin warp imaging this splitting is not significant because of the large pixel bandwidth. However, in echo planar images the effective pixel bandwidth along the phase-encoded direction is in general small, resulting in a frequency range per pixel that is less than a typical one bond coupling constant. The effect of the coupling Hamiltonian must therefore be removed to avoid ^{13}C EP image artefacts. Two different strategies for achieving this are presented here.

Eliminating the Effect of J-Coupling during a Single EPI Acquisition

The simplest sequence for removing the effect of J-coupling during the EPI acquisition involves the application of a train of 180° pulses applied to the ^{13}C nuclei, thus repetitively refocusing the evolution under the effect of the J-coupling. The 180° pulses are best applied during each zero-crossing of the oscillating readout gradient as shown in sequence (a) of Fig. 2. An additional ^{13}C 180° pulse was applied between the end of the CYCLCROP module and the beginning of the EPI acquisition, to ensure that the effect of the J-coupling was refocused at the first echo. This pulse was issued at a time t_a after the end of the

CYCLCROP module, given by

$$t_a = \frac{T_E}{4} - \frac{t_b}{2}, \quad [1]$$

where T_E is the echo time, and t_b is the time between the application of the slice-selective 180° pulse on the ^{1}H channel and the first 180° pulse applied on the ^{13}C channel minus half the time between adjacent echoes during the EPI acquisition.

Suppressing the Effect of J-Coupling with Two EPI Acquisitions

In an alternative approach, images unaffected by the J-coupling between ^{1}H and ^{13}C nuclei may be formed from the data acquired in two independent experiments using a version of the CYCLCROP EPI sequence incorporating a single ^{1}H 180° RF pulse and a single ^{13}C 180° RF pulse before the EPI module, as shown in Sequence b of Fig. 2. While the timing of the ^{1}H 180° RF pulse is kept constant, the ^{13}C 180° RF is applied at different times after the end of the CYCLCROP module in the two experiments. In the first experiment, the ^{13}C 180° RF pulse is applied immediately after the end of the CYCLCROP module. The action of the ^{1}H 180° RF pulse means that the signals from the two components of the doublet are in phase a time T_E later, when data at the center of k-space are acquired. In the second experiment, the application of the ^{13}C 180° RF pulse is delayed by a time $(4J)^{-1}$. This means that the signal from the two components is in anti-phase at the center of k-space and 90° out of phase with the signal acquired in the first experiment. Addition and subtraction of the two data sets, following an appropriate zero-order phase correction, yield images separately showing the two components of the doublet. These two images are shifted relative to one another in the phase encode direction by JT pixels, where T is the duration of the echo train in the EPI data acquisition. The complex images were therefore subsequently shifted in the phase direction to compensate for the frequency difference and then added together. Through this postprocessing procedure an image unaffected by the coupling Hamiltonian can be obtained with the full image SNR, but using only one additional RF pulse.

Field Mapping Using the CYCLCROP–EPI Sequence

For optimal transfer efficiency in a Hartmann–Hahn experiment it is crucial to apply highly uniform and matched B_1 fields across the sample, since the transfer efficiency typically falls to less than 50% for $|(\gamma B_1)^{13C} - (\gamma B_1)^{1H}| > \pi J$ (*3*), where in the case of PRAWN the terms in brackets represent the average value of γB_1. Accurate knowledge of the spatial uniformity of the B_1 field generated at both the ^{13}C and ^{1}H NMR frequencies is therefore important. B_1 field maps may be conveniently generated using image-based mapping techniques. One such technique, introduced by Talagala and Gillen (*20*), uses a series of images, acquired with a progressively increasing RF excitation pulse flip angle, with the B_1 field strength being obtained by Fourier transformation of the resulting signal modulation in the image series. However, direct imaging of nuclei of low magnetogyric ratio is impractical because of the long experimental duration that is required to give adequate SNR. The CYCLCROP-EPI sequence may be used to overcome this sensitivity limitation and to yield B_1 maps in relatively short acquisition times. Here, a modified variant of the Talagala and Gillen method (*20*) was used to map the B_1 field strength at the ^{13}C resonance frequency. This involved modifying the CYCLCROP-EPI sequence, so that the duration of the ^{13}C storage RF pulse, applied after the first polarization transfer module (Fig. 1), was incremented after each image acquisition. The pixel intensity in the resulting set of carbon-edited proton images consequently varies sinusoidally with the pulse length, at a frequency proportional to the ^{13}C B_1-field strength. It should be noted, however, that zero quantum coherences which survive the saturation module on the proton channel can lead to minor deviations from this behaviour. Since this method uses frequency modulation to encode B_1-field information, it is not strongly sensitive to the absolute local signal intensity (*20*). This means that sample regions exhibiting suboptimal Hartmann–Hahn matching or reduced signal due to relaxation effects will also be mapped, provided that there is sufficient image SNR. This method was applied to mapping the B_1-field generated at the ^{13}C NMR frequency by a 16-mm-diameter double-birdcage coil, comprising a low-pass 8-rung structure tuned to 125 MHz and a high-pass 8-rung structure tuned to 500 MHz (*21*). This RF coil was employed in all the experiments carried out at 11.7 T.

RESULTS

CYCLCROP–EPI Imaging

Figure 3 shows a 64 × 64 EP image of a phantom containing 400 mM ^{13}C-1-glucose in water which was generated in 1.4 s using the CYCLCROP-EPI sequence applied at 11.7 T, using the method of Fig. 2a to eliminate the effect of J-coupling. The image was constructed from two signal acquisitions employing a $(y, -y)$ phase cycle of the ^{13}C 90° read back pulse and ^{1}H receiver phase, prior to the second Hartmann–Hahn mixing module, to suppress further the signal from uncoupled ^{1}H nuclei. The carrier frequencies of the RF pulses were set to the resonance of the more abundant anomeric carbon atom of ^{13}C-1β-glucose. In equilibrium, the fraction of the β-glucose anomer is 65% (260 mM). The technique is sufficiently frequency selective so that the resonance of the anomeric carbon of 140 mM ^{13}C-1α-glucose is completely suppressed (the two proton signals are split by 0.58 ppm, which is 290 Hz at 11.7 T). The image SNR (central signal intensity divided by the standard deviation of a noise region) is only approximately 17, but this is achieved with 1.76 μl voxel volume and an effective ^{1}H spin density which is 416 times less than the ^{1}H spin density of water. For comparison, Fig. 3b shows a spin-warp, ^{13}C image acquired from the same

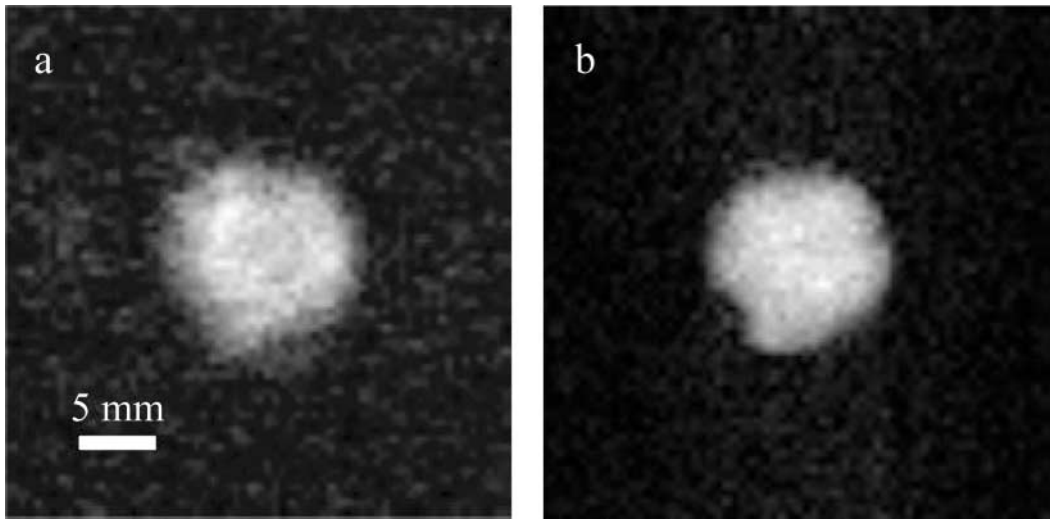

FIG. 3. (a) A CYCLCROP-EP image acquired at the β-$^{13}C_1$-glucose resonance. The sample consisted of a 12-mm-diameter tube containing 400 mM $^{13}C_1$-glucose (267 mM with respect to the β-$^{13}C_1$-resonance). The image matrix is 64×64, with a 38×38-mm FOV and 5-mm slice thickness ($T_E = 15.4$ ms; $T_R = 0.7$ s) and the image was acquired in 1.4-s, using a two-step phase cycle. (b) A CYCLCROP-2DFT image of the same sample with the same FOV and slice thickness, T_R and T_E acquired in 100 s, using a two-step phase cycle.

sample in a time of 1.7 min, using PRAWN-based CYCLCROP. This image displays some signal loss at the sample periphery, which is also present in the echo planar image. This loss results from local Hartmann–Hahn mismatch, due to RF inhomogeneity close to the struts of the 16-mm-diameter ^{13}C and ^{1}H bird-cage RF coils.

Eliminating the Effect of J-Coupling in EP Images

A two-compartment phantom was constructed using a 5-mm NMR tube placed centrally within a 12-mm NMR tube. The central 5-mm tube was filled with unlabeled methanol, while the outer tube was filled with 50% ^{13}C-labeled methanol. Figure 4a shows an un-decoupled CYCLCROP-echo planar (EP) image of this phantom. The central tube does not appear in the image, indicating good suppression of the signal from the ^{1}H nuclei that are not coupled to those of ^{13}C. The signal from the 1.1% natural-abundance ^{13}C-methanol in the inner tube was not detected above the level of noise and signal artefact. The two rings in this figure result from the frequency splitting (140 Hz) of the ^{1}H resonance, which is manifested as image separation along the vertical phase-encode direction of the EP image. When 180° ^{13}C RF refocusing pulses are applied at each gradient crossing of the switched gradient, the two rings collapse into a single image, as shown in Fig. 4b.

Images acquired using the second technique to suppress the effect of the coupling Hamiltonian are shown in Figs. 4c–g. Figure 4d was generated by delaying the 180° ^{13}C RF pulse by $(4J)^{-1}$ after the final polarization transfer module, thus introducing an additional $(2J)^{-1}$ time evolution under the action of the J coupling when compared to the image in Fig. 4c. The sum of these two images is displayed in Fig. 4e, and the difference is shown in Fig. 4f. The images in Figs. 4e and f show the two data sets corresponding to the higher and lower frequencies of the ^{1}H signal doublet. As the magnitude of the J-coupling is known, the images may be shifted accordingly and then coadded to yield the final image shown in Fig. 4g. This provides an image in which the effect of the J-coupling is suppressed, via the addition of only one 180° ^{13}C RF pulse to the CYCLCROP-EPI sequence. This offers a significant advantage when sample RF power deposition in an experiment is an issue, as for example in *in vivo* studies.

The performance of the CYCLCROP-EPI sequence was further tested in an experiment designed to investigate the transport and accumulation of ^{13}C-labeled sucrose in the vascular bundles of a castor bean seedling (*Ricinus communis* L.). The castor bean plant was accommodated in a purpose-designed probe head that could be inserted into a Bruker microimaging gradient tube. During the experiments, the roots of the hydroponically grown plant were aerated from below and the cotyledons were immersed in a small vessel containing 50 mM ^{13}C-1-labeled glucose and ^{13}C-1-labeled fructose (*5*).

In this experiment, which was carried out on a Bruker microimaging system at 9.4 T, an EPI sequence with 24 echoes and 64 sampling points per echo was employed. Figure 5a shows an image acquired with the CYCLCROP-EPI sequence from 1600 averaged acquisitions. For comparison, an image acquired with the CYCLCROP spin-warp technique (*5*) is shown in Fig. 5b and a standard ^{1}H-spin-warp image is shown in Fig. 5c. In the CYCLCROP spin-warp experiment, k-space was sampled in 16 increments in the phase-encoding direction and with 64 points in the read-gradient direction. Total acquisition times for the CYCLCROP-EPI and spin-warp imaging experiments were 16 and 85 min respectively. In both images seven vascular bundles

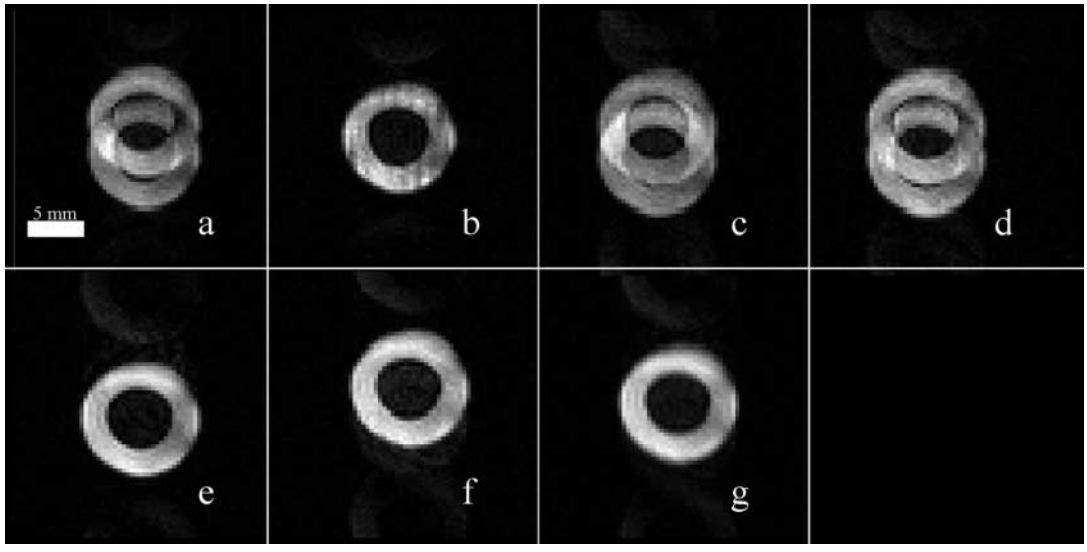

FIG. 4. ^{1}H detected ^{13}C echo-planar images of a phantom consisting of a central, 5-mm-diameter tube containing unlabeled methanol, inside a 12-mm-diameter tube containing ^{13}C-labeled methanol. In all images the slice thickness is 5 mm and the FOV 25 × 25 mm . Images are averages of 16 acquisitions using a 2-step phase cycle ($T_R = 5$ s, $T_E = 60$ ms) The PRAWN contact time was 3.57 ms and the phase encode pixel bandwidth (vertical direction on the images) was 17.7 Hz. (a) ^{1}H detected, ^{13}C image, acquired without ^{13}C 180° RF refocusing pulses. (b) ^{1}H detected, ^{13}C acquired using multiple ^{13}C 180° RF refocusing pulses. (c) ^{1}H detected, ^{13}C image acquired using a single ^{13}C 180° RF pulse applied immediately after the CYCLCROP module. (d) ^{1}H detected, ^{13}C image acquired using a single ^{13}C 180° RF pulse shifted by a time $1/4J$ relative to the sequence used in (c). (e) The sum of images (c) and (d) (using an additional zero order phase correction to the time data of (d) in order to optimize cancellation) representing the signal from one resonance of the split proton doublet. (f) The difference of images (c) and (d) (using an additional zero-order phase correction to the time data of (d) in order to optimize cancellation) representing the signal from the other resonance of the split proton doublet. (g) Carbon-edited proton detected SE-MBEST image, calculated by shifting images (e) and (f) toward the center in the phase encode direction by 3.7 pixels and then adding.

appear with bright intensities due to high concentration of ^{13}C-labeled sucrose in this tissue. The absence of signal from the eighth bundle may result from lower uptake in this tissue, but most probably is an artefact resulting from RF mismatch due to the ^{1}H RF inhomogeneity, which is also manifested in the region of lower intensity on the right-hand side of the ^{1}H image. Despite this effect, the CYCLCROP-EPI experiment clearly provides similar information about the signal intensity in the vascular bundles on a much shorter time scale than the 2DFT imaging. Therefore, this technique will be useful if dynamic

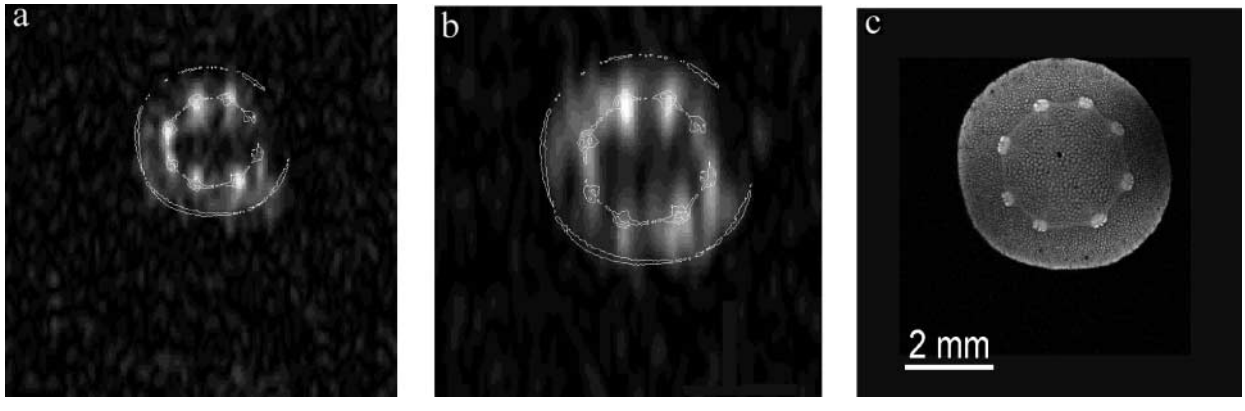

FIG. 5. Metabolite mapping in a 6-day-old castor bean seedling. (a) CYCLCROP-EPI image of ^{13}C-labeled sucrose. The image matrix is 64 × 24, with a 7 × 7 -mm FOV and 5-mm slice thickness. The image was acquired in 16 min, using a two-step phase cycle. ($T_R = 0.6$ s, number of scans = 1600.) The contours on the image marking the position of the vascular bundles and the outer surface of the cotyledon were produced by applying edge detection to the conventional ^{1}H image shown in (c). (b) A spin–echo, CYCLCROP image of ^{13}C-labeled sucrose. The image matrix is 64 × 16, with a 7 × 7-mm FOV and 5-mm slice thickness. The image was acquired in 85 min, using a k-space Hanning filter. ($T_R = 0.8$ s; maximum number of averages = 400 at the center of k-space.) Contours produced as in (a). (c) A spin–echo ^{1}H image of a transverse plane through the hypocotyl of a castor bean seedling. The image matrix is 256 × 256, with a 7 × 7-mm FOV and 1-mm slice thickness. The image was acquired in 42 min, using a two-step phase cycle. ($T_R = 5$ s, $T_E = 6$ ms, number of scans = 16.)

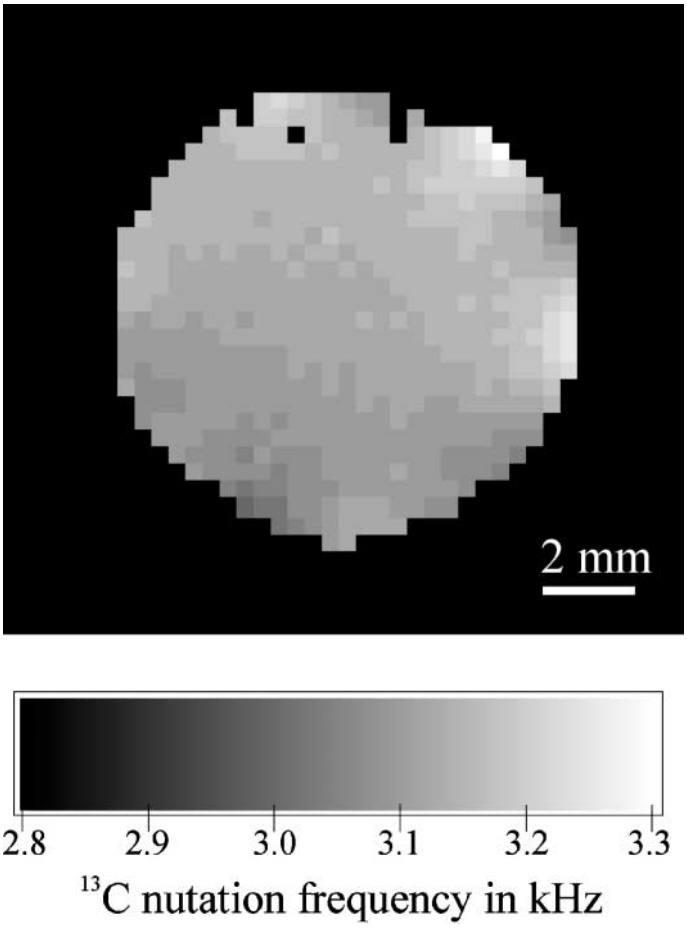

FIG. 6. ^{1}H detected, axial ^{13}C B_1 field map taken using a 10 mm diameter tube containing 50% enriched ^{13}C-methanol inside a 16-mm-diameter double-resonant birdcage coil. Slice thickness 5 mm. Image matrix size 64 × 64. Generated from data produced by Fourier transformation of 64, SE-MBEST images (zero filled to 512), sequentially acquired using the sequence of Fig. 2a, with an incremented length of the ^{13}C B_1 encoding duration (using a 30-μs pulse length increment). Repetition time 1 s. The B_1 field intensity is displayed in units of ^{13}C nutation frequency.

processes with comparatively short time constants are to be observed. However, the signal intensity of ^{13}C-labeled sucrose in the surrounding tissue is attenuated in the CYCLCROP-EPI image. This effect results from the high sensitivity of the EPI sequence to rapid signal decay due to short T_2^* time constants.

Field Mapping Using the CYCLCROP–EPI Sequence

A set of 64 axial, proton-detected ^{13}C EPI images were generated using a 10-mm-diameter, 50% enriched ^{13}C-methanol sample, placed inside the 16-mm-inner-diameter double birdcage coil system (*21*) at 11.7 T. The images were acquired with a 5-mm slice thickness, a 64 × 64 matrix size, and a repetition time of 1 s. The duration of the ^{13}C RF storage pulse was increased by 30 μs per image. The data were exponentially filtered and zero-filled to 512 points in the B_1 encoding direction. After three-dimensional Fourier transformation, a quantitative B_1-field map was obtained by extracting the spatially dependent frequency from the B_1 encoding direction in the data set and is shown in Fig. 6. The resulting data are in good agreement with a similar map acquired using PRAWN-based CYCLCROP in conjunction with a spin-warp imaging procedure (*21*). The EPI data were, however, acquired in just 64 s, compared with a 68 min acquisition time for the spin-warp sequence. These data were used in conjunction with maps of the ^{1}H B_1 homogeneity and the B_0 field variation to calculate the spatial variation of the Hartmann–Hahn transfer efficiency for the 16-mm-diameter double-birdcage coil system. The results indicate that with the average B_1 field set to 250 Hz the one-way transfer efficiency varies by less than 5% over a central 10-mm-diameter field of view in the central slice, assuming a perfectly homogeneous ^{1}H RF field .

CONCLUSION

The CYCLCROP-EPI sequence allows images representing the spatial distribution of ^{13}C in particular chemical environments to be generated with high sensitivity and short scan times. Therefore, this technique offers the possibility of mapping the temporal evolution of the distribution of selected ^{13}C-labeled metabolites. Phantom images with reasonable SNR have been acquired in less than 2 s. The combination of echo planar imaging with cyclic polarization transfer makes efficient use of the available signal. This permits the experiment to be designed with either a higher temporal or spatial resolution, depending on the application and relaxation properties of the sample. With less efficient, slower imaging sequences (for example, spin-warp based imaging), this is not an option; the long scan time dictates the achievable temporal resolution. The use of CYCLCROP provides high spectral selectivity, along with excellent water suppression. The latter is achieved by exciting and crushing all ^{1}H magnetization, while the polarization of interest is stored as longitudinal ^{13}C magnetization. In conjunction with the use of echo–planar acquisition this should make the sequence very insensitive to motion, which may cause incomplete subtraction of signals in difference-based sequences, particularly when phase encoding is employed.

In contrast to spin-warp imaging with short T_E values, the MBEST EPI sequence can introduce additional T_2^* contrast. This additional T_2^* weighting of the indirectly detected ^{13}C signal can be minimized by using modifications of the EPI sequence which allow early sampling of the center of k-space. Such modifications include half-Fourier EPI or spiral EPI (*7*). Other effects which may limit the ability of the sequence to provide quantification include RF or main magnetic field inhomogeneity leading to Hartmann–Hahn mismatch and a consequent reduction in the efficiency of polarization transfer (*11*), as well as voxel bleeding in the case of small image matrix sizes (*22*).

Two methods for suppressing the effect of the coupling interaction between ^{1}H and ^{13}C spins during EPI signal acquisition

have been implemented. One method allows single-shot imaging via application of a train of RF refocusing pulses applied on the ^{13}C channel at the zero-crossings of the oscillating read gradient used in EPI. This single-shot technique will be most useful in experiments where high concentrations of labeled compound are available and a high temporal resolution is desirable. The second, two-shot method requires postprocessing, but uses only one additional RF pulse, and is therefore preferred in applications where RF power deposition is an issue.

REFERENCES

1. N. Beckmann, "^{13}C NMR Spectrosocopy of Biological Systems," Academic Press, San Diego (1995).
2. C. Kunze and R. Kimmich, Proton-detected ^{13}C imaging using cyclic J cross polarization, *Magn. Reson. Imaging* **12,** 805–810 (1994).
3. R. Kimmich, "NMR Tomography Diffusometry Relaxometry," Springer-Verlag, Berlin (1997).
4. M. Heidenreich, A. Spyros, W. Köckenberger, N. Chandrakumar, R. Bowtell, and R. Kimmich, CYCLCROP mapping of ^{13}C labeled compounds: Perspectives in spatially polymer science and plant physiology, *in* "Spatially Resolved Magnetic Resonance" (P. Blumler, B. Blumich, R. Botto, and E. Fukushima, Eds.), Wiley/VCH, Weinheim (1998).
5. M. Heidenreich, W. Köckenberger, R. Kimmich, N. Chandrakumar, and R. Bowtell, Investigation of carbohydrate metabolism and transport in castor bean seedlings by cyclic J cross polarisation imaging and spectroscopy, *J. Magn. Reson.* **132,** 109–124 (1998).
6. A. Haase, J. Frahm, D. Matthaei, W. Hanicke, and K. D. Merboldt , FLASH imaging—Rapid NMR imaging using low flip-angle pulses. *J. Magn. Reson.* **67,** 258–266 (1986).
7. P. A. Wielopolski, F. Schmitt, and M. K. Stehling, Echo planar imaging pulse sequences, *in* "Echo-Planar Imaging" (F. Schmitt, M. K. Stehling, and R. Turner, Eds.), Springer-Verlag, Berlin (1998).
8. M. Heidenreich, W. Köckenberger, N. Chandrakumar, R. Bowtell, and R. Kimmich, Investigation of carbohydrate transport and metabolism in plants by indirect 13C imaging and spectroscopy, *in* "EENC Abstracts, Bled, 1998."
9. W. Chen, G. Adriany, X.-H. Zhu, R. Gruetter, and K. Ugurbil, Detecting natural abundance carbon signal of NAA metabolite within 12-cm^3 localized volume of human brain using ^{1}H–{^{13}C} NMR spectroscopy, *Magn. Reson. Med.* **40,** 180–184 (1999).
10. D. L. Rothman, E. J. Novotny, G. I. Shulman, A. M. Howseman, O. A. Petroff, G. Mason, T. Nixon, C. C. Hanstock, J. W. Prichard, and R. G. Shulman, ^{1}H–{^{13}C} NMR measurements of [4-^{13}C] glutamate turnover in human brain, *Proc. Natl. Acad. Sci.* **89,** 9603–9606 (1992).
11. N. Chandrakumar and R. Kimmich, PRAWN: Mixing sequences for selective heteronuclear J cross polarization, *J. Magn. Reson.* **137,** 100–107 (1999).
12. D. N. Guilfoyle, A. Blamire, B. Chapman, R. J. Ordidge, and P. Mansfield, PEEP—A rapid chemical shift imaging method, *Magn. Reson. Med.* **10,** 282–287 (1989).
13. F. Hyder, R. Renken, and D. L. Rothman, *In vivo* carbon-edited detection with proton echo-planar spectroscopic imaging (ICED-PEPSI): [3, 4-$^{13}CH_2$] glutamate/glutamine tomography in rat brain, *Magn. Reson. Med.* **42,** 997–1003 (1999).
14. S. Morikawa and T. Inubushi, Fast ^{13}C-glucose metabolite mapping in rat brain using ^{1}H echo planar spectroscopic imaging technique at 2 T, *J. Magn. Reson. Imaging* **13,** 787–791 (2001).
15. M. R. Bendall and D. T. Pegg, Uniform sample excitation with surface coils for *in vivo* spectroscopy by adiabatic rapid half passage, *J. Magn. Reson.* **67,** 376–381 (1986).
16. K. Woelk and J. W. Rathke, Composite 90° and 180° pulses to compensate for radiofrequency gradients in toroid NMR detectors, *J. Magn. Reson. A* **115,** 106–115 (1995).
17. N. Chandrakumar, Restoring natural multiplet patterns in J-cross polarization spectra, *J. Magn. Reson.* **63,** 202–206 (1985).
18. G. C. Chingas, R. D. Bertrand, A. N. Garroway, and W. B. Moniz, Determination of NMR spin coupling constants using J-cross polarization: A comment on "J-cross polarization in silanes," *J. Am. Chem. Soc.* **101,** 4058–4059 (1979).
19. A. M. Howseman, M. K. Stehling, B. Chapman, R. Coxon, R. Turner, R. J. Ordidge, M. G. Cawley, P. Glover, P. Mansfield, and R. E. Coupland, Improvements in snapshot nuclear magnetic-resonance imaging, *Br. J. Radiol.* **61,** 822–828 (1988).
20. S. L. Talagala and J. Gillen, Experimental determination of three-dimensional RF magnetic field distribution of NMR coils, *J. Magn. Reson.* **94,** 493–500 (1991).
21. A. M. J. Hudson, W. Köckenberger, and R. W. Bowtell, Dual resonant birdcage coils for ^{1}H detected ^{13}C microscopic imaging at 11.7 T, *MAGMA* **10,** 61–68 (2000).
22. T. Koch, G. Brix, and W. J. Lorenz, Theoretical description, measurement and correction of localization errors in ^{31}P chemical-shift imaging, *J. Magn. Reson. B* **104,** 199–211 (1994).